Magnetic and Electronic Properties in Novel Terpyridine-Based Nitroxide Complexes: Strong Radical−Metal Interaction via a Pyridyl Ring

Christophe Stroh,[†] Philippe Turek,[‡] Pierre Rabu,[#] and Raymond Ziessel*[,†]

Laboratoire de Chimie, d'Electronique et de Photonique Moléculaires, Ecole de Chimie, Polymères et Matériaux (ECPM), UPRES-A 7008, Université Louis Pasteur (ULP), 25, rue Becquerel, 67087 Strasbourg Cedex 2, France, Institut Charles Sadron, Université Louis Pasteur (ULP), 6, rue Boussingault, 67083 Strasbourg Cedex, France, and Institut de Physique et de Chimie de Strasbourg, Groupe de Matériaux Inorganiques, 23 rue du Loess, 67037 Strasbourg Cedex, France

Received December 28, 2000

Transition metal complexes of 2-[4′-(2,2′:6′,2″-terpyridyl)]-(4,4,5,5-tetramethylimidazolinyl-3-oxide-1-oxyl) (terpy-NIT) and 2-[4′-(2,2′:6′,2″-terpyridyl)]-(4,4,5,5-tetramethylimidazolinyl-1-oxyl) (terpy-IM) have been prepared. Whereas the pyridyl fragments of the free ligands are in an anti conformation, the complexes are obtained by coordination of two terpyridines in a syn conformation, forming a distorted octahedron around the metal center: $[M(terpy\text{-}NIT)_2](ClO_4)_2$ (M = Ni(II) **1**, Zn(II) **2**, Cu(II) **3**) and $[M(terpy\text{-}IM)_2](ClO_4)_2$ (M = Ni(II) **4**, Zn(II) **5**). The ligands and their complexes have been characterized by FAB-MS, UV−vis, FT-IR spectroscopies, elemental analysis, and by EPR spectroscopy and susceptibility measurements. Single-crystal X-ray diffraction have been performed on the terpy-NIT ligand and on complexes **1**, **4**, and **5** giving following crystal data: terpy-NIT, monoclinic, $P2_1/c$, Z = 4, a = 14.2186(5), b = 12.9129(6), c = 11.704(1) Å, β = 108.615(4)°; **1**, orthorhombic, P(n a 2_1), Z = 4, a = 23.6367(6), b = 8.7836(1), c = 24.2748(7) Å; **4**, monoclinic, $P2_1$, Z = 1, a = 8.738(1), b = 25.010(1), c = 11.704(1) Å, β = 102.849(3)°; **5**, monoclinic, $P2_1$, Z = 1, a = 8.7463(2), b = 25.0833(5), c = 11.8168(3) Å, β = 102.757(3)°. For complexes **1** and **3**, an antiferromagnetic behavior has been found and parametrized by considering a symmetric magnetic trimer, highlighting a strong intramolecular coupling between the metal and the radicals (average values $2J_{M-NIT} = -19.6$ K for M = Ni and −22.8 K for M = Cu). In the case of compound **4**, an asymmetric magnetic trimer has been used to model the antiferromagnetic interactions ($2J_{Ni-IM1} = -13.0$ K, $2J_{Ni-IM2} = -5.6$ K). The shape of the EPR spectra of complexes **2**, **3**, and **5** in solution indicates the intermediate exchange limit, of the order of a few mK, between the two nitroxide radicals through the pyridyl−metal−pyridyl fragment.

Introduction

The design and synthesis of magnetic materials is an attracting research area.[1,2] One fascinating target in this field rely on molecular-based magnets that exhibit spontaneous magnetization. Spectacular results have been provided by the Prussian-Blue family of compounds which show spontaneous magnetization and high magnetic ordering temperatures.[3−6] Recently, versatile synthetic methods have provided numerous high-spin molecules[7−9] and metal assemblies of ordered networks.[10] Another possible way to construct high-spin molecules may rely on the use of polyradicals as modules interacting magnetically via coupling units.[11] Many different radicals have been studied but one of the most famous is Ullman's nitronyl-nitroxide widely used for its simplicity of synthesis, its stability, and its ability to generate cooperative magnetic properties.[12] In fact, the first purely organic ferromagnet is based on the β cristalline phase of *p*-nitrophenyl-nitronyl-nitroxide.[13] Furthermore, nitronyl-nitroxides (NIT) and their imino-nitroxide (IM) derivatives are also used in the so-called hybrid strategy, which combines them with transition metals to obtain different interaction schemes as observed in multinuclear scaffoldings.[14] Nevertheless, in the absence of additional donor group, the low basicity of such radicals allows only the complexation of acidic metal centers, bearing sterically crowded ligands such as hexafluoroacetyl-acetonates. This stimulated some chemists to design and prepare coordinating ligands bearing nitronyl-nitroxides, to avoid the

* To whom correspondence should be sent.
[†] Ecole de Chimie, Polymères et Matériaux, Université Louis Pasteur.
[‡] Institut Charles Sadron, Université Louis Pasteur.
[#] Institut de Physique et de Chimie de Strasbourg.

(1) Kahn, O. *Molecular Magnetism*; VCH: New York, 1993.
(2) *Molecular Magnetism: From Molecular Assemblies to the Devices*; Coronado, E., Delhaès, P., Gatteschi, D., Miller, J. S., Eds.; NATO ASI Series E 321; Kluwer Academic Publishers: Dordrecht, 1996.
(3) Miller, J. S.; Epstein, A. J.; Reiff, W. M. *Chem. Rev.* **1988**, *88*, 201.
(4) Ferlay, S.; Mallah, T.; Ouahés, R.; Veillet, P.; Verdaguer, M. *Nature* **1995**, *378*, 701.
(5) Hatlevik, Ø.; Buschmann, W. E.; Zhang, J.; Manson, J. L.; Miller, J. S. *Adv. Mater*. **1999**, *11*, 914 and references therein.
(6) Ohba, M.; Usuki, N.; Fukita, N.; Okawa, H. *Angew. Chem., Int. Ed*. **1999**, *38*, 1795 and references therein.
(7) Iwamura, H.; Koga, N. *Acc. Chem. Res.* **1993**, *26*, 346; Rajca, A. *Chem. Rev*. **1994**, *94*, 871; Rajca, A.; Rajca, S. *J. Am. Chem. Soc*. **1996**, *118*, 8121.
(8) Vostrikova, K. E.; Luneau, D.; Werndorfer, W.; Rey, P.; Verdaguer, M. *J. Am. Chem. Soc*. **2000**, *122*, 718.
(9) Larionova, J.; Gross, M.; Pilkington, M.; Andres, H.; Stoechli-Evans, H.; Güdel, H. U.; Decurtins, S. *Angew. Chem., Int. Ed*. **2000**, *39*, 1605.
(10) De Munno, G.; Julve, M.; Viau, G.; Lloret, F.; Faus, J.; Viterbo, D. *Angew. Chem., Int. Ed*. **1996**, *35*, 1807. De Munno, G.; Poerio, T.; Viau, G.; Julve, M.; Lloret, F.; Yournaux, Y.; Rivière *Chem. Commun*. **1996**, 2587.
(11) Ziessel, R. *Synthesis* **1999**, 1839.
(12) Osiecki, J. H.; Ullman, E. F. *J. Am. Chem. Soc*. **1968**, *90*, 1078.
(13) Tamura, M.; Nakasawa, Y.; Shiomi, D.; Nozawa, K.; Hosokoshi, Y.; Ishikawa, M.; Takahashi, M.; Kinoshita, M. *Chem. Phys. Lett*. **1991**, *186*, 401.
(14) Lippard, S. J. Progress *Inorg. Chem*. **1991**, *39*, 329. Caneschi, A.; Gatteschi, D.; Sessoli, R. *Acc. Chem. Res*. **1989**, *22*, 392.

10.1021/ic001473+ CCC: $20.00
Published on Web 09/11/2001

Table 1. Summary of the Crystal Structure Data Collection and Refinement for **1**, **4**, and **5**

	Terpy-NIT	**1**	**4**	**5**
formula	$C_{22}H_{22}N_5O_2$	$C_{44}H_{44}N_{10}O_4Ni\cdot 2ClO_4\cdot CH_2Cl_2\cdot H_2O$	$2(C_{44}H_{44}N_{10}O_2Ni)\cdot 4ClO_4\cdot 2CH_2Cl_2\cdot CH_3OH$	$2(C_{44}H_{44}N_{10}O_2Zn)\cdot 4ClO_4\cdot 2CH_2Cl_2\cdot CH_3OH$
fw	388.45	1137.47	2206.95	2220.27
temp (K)	294	173	173	173
cryst syst	monoclinic	orthorhombic	monoclinic	monoclinic
space group	$P\,1\,2_1/c\,1$	$P\,n\,a\,2_1$	$P\,1\,2_1\,1$	$P\,1\,2_1\,1$
Z	4	4	1	1
a (Å)	14.2186(5)	23.6367(6)	8.738(1)	8.7463(2)
b (Å)	12.9129(6)	8.7836(1)	25.010(1)	25.0833(5)
c (Å)	11.704(1)	24.2748(7)	11.704(1)	11.8168(3)
α (deg)	90	90	90	90
β (deg)	108.615(4)	90	102.849(3)	102.757(3)
γ (deg)	90	90	90	90
V (Å^3)	2036.5(4)	5039.8(3)	2493.7(6)	2528.4(2)
Dc (g·cm^{-3})	1.27	1.50	1.47	1.46
μ (Mo Kα) (mm^{-1})	0.079	0.669	0.671	0.764
GOF[a]	1.459	1.583	1.033	1.132
R (F_o)[b]	0.049	0.067	0.050	0.049
R_w (F_o)[c]	0.073	0.082	0.067	0.069

[a] GOF $= [\sum w(|F_o|^2 - |F_c|^2)2/(n-p)]^-$. [b] $R(F_o) = \sum(|F_o| - |F_c|)/\sum|F_o|$. [c] $R_w(F_o) = \sum(w - |F_o| - |F_c|)/\sum w - |F_o|$.

Chart 1. Molecular Structures of the (terpy-NIT) and (terpy-IM) Ligands

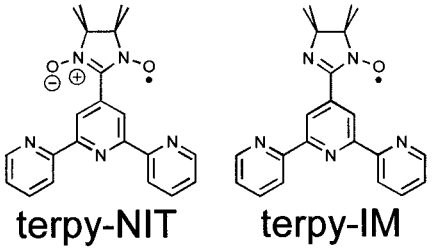

use of these bulky acidic metal ions and to build new molecular arrangements. Some ligands used for this purpose are pyridine[15] and bipyridine frames functionalized with nitroxide radicals.[16] In most cases the radical fragment is grafted in such a way that coordination of the radical to the metal center occurs. To our knowledge, only few examples of magnetic interactions between nitronyl-nitroxides and a metal center ion via a pyridyl ring have been reported.[17] Sometimes, complicated coordination scheme has been provided with copper(II) complexes formed by coordination of a pyridine ligand graphted in meta position with a NIT radical.[18]

Herein, we wish to report the use of terpyridine ligands bearing nitronyl-nitroxide (terpy-NIT) or imino-nitroxide (terpy-IM) radicals to form [Ni(II)(terpy-NIT)$_2$], [Ni(II)(terpy-IM)$_2$], and [Cu(II)(terpy-NIT)$_2$] complexes (Chart 1). The diamagnetic Zn(II) complexes have also been prepared as test compounds. To the best of our knownledge there is no detailed study concerning transition metal complexes of terpyridine chelates bearing an Ullman's radical. We fill here the gap and evidence some significant intramolecular magnetic interactions between the organic radical and the paramagnetic metal via the central pyridine ring. Furthermore, the present work reveals the exchange interaction, although very weak between two organic radicals via a pyridyl−metal−pyridyl moiety.

Experimental Section

X-ray Crystal Structure Analysis. The intensity data were collected in the phi scan mode, at 294 K on a MACH3 Nonius diffractometer for the ligand or at 173 K on a KappaCCD diffractometer for the complexes, equipped with a graphite monochromator for the Mo Kα radiation. Cell constants were derived from a least-squares fit of the setting angles for 25 selected reflections with $10° < \theta < 15°$. The intensities were corrected for Lorentz and polarization effects but not for absorption. The positions of the metal ions were found using the SHELX86 package.[19] The remaining atoms were located in a succession of difference Fourier syntheses and were refined with anisotropic thermal parameters using the SHELX76 package.[20] The hydrogen atoms were included in the final refinement model in calculated and fixed positions with isotropic thermal parameters. Crystal structure and refinement data are summarized in Table 1.

Magnetic Susceptibility Measurements. The magnetic susceptibility was measured on the bulk polycrystalline material in the 2−300 K temperature range for each compound with a Quantum Design MPMS superconducting SQUID magnetometer operating at a field strength of 5 kOe or with a M 8100 SQUID susceptometer Métronique at field strength of 1 kOe. The data were corrected for magnetization of the sample holder and the magnetic susceptibilities were corrected for the diamagnetism inherent to the molecules by fitting the high-temperature data of the $\chi\cdot T$ versus T curve.

EPR Measurements. The EPR spectra were recorded at X-band (ca. 9.8 GHz) with a Bruker ESR 300 spectrometer equipped with a rectangular TE 102 cavity. A continuous flow ESR 900 cryostat supplied by Oxford Instruments was inserted into the cavity for low-temperature measurements down to 4 K. The solid samples (powders) were inserted in calibrated 3.5 inner diameter EPR quality quartz tubes. An alternative experimental setup was provided for fluid solutions by using thin capillary tubes with ca. 1 mm outer diameter.

Other Instrumentation. UV−vis spectra: Uvikon 933 (Kontron Instruments) spectrophotometer. FT-IR spectra: Bruker IFS 25 spectrometer; KBr pellets. Fast-atom bombardment (FAB, positive mode) ZAB−HF−VG-Analytical apparatus in a *m*-nitrobenzyl alcohol (*m*-NBA) matrix.

Materials. Perchlorate salts were used as purchased. *Perchlorate salts should be handled carefully, in low quantities, as hydrated salts,*

(15) Caneschi, A.; Ferraro, F.; Gatteschi, D.; Rey, P.; Sessoli, R. *Inorg. Chem.* **1990**, *29*, 4217.
(16) Luneau, D.; Romero, F. M.; Ziessel, R. *Inorg. Chem.* **1998**, *37*, 5078.
(17) (a) Caneschi, A.; Gatteschi, D.; Sessoli, R.; Rey, P. *Inorg. Chim. Acta* **1991**, *184*, 67. (b) Caneschi, A.; Ferraro, F.; Gatteschi, D.; Rey, P.; Sessoli, R. *Inorg. Chem.* **1993**, *32*, 5616. (c) Chen, Z. N.; Qiu J.; Gu, J. M.; Wu, M. F.; Tang, W. X. *Inorg. Chim. Acta* **1995**, *233*, 131. (d) Fettouhi, M.; Khaled, M.; Waheed, A.; Golhen, S.; Ouahab, L.; Sutter, J.-P.; Kahn, O. *Inorg. Chem.* **1999**, *38*, 3967.
(18) Lanfranc de Panthou, F.; Luneau, D.; Musin, R.; Öhrström, L.; Grand, A.; Turek, P.; Rey, P. *Inorg. Chem.* **1996**, *35*, 3484.
(19) Sheldrick, G. M. *Crystallographic Computing 3*; Sheldrick, G. M., Kruger, C., Goddard, R., Eds.; Oxford University Press: Oxford, U.K., 1985; p 175.
(20) Sheldrick, G. *System of Computing Programs*; University of Cambridge: England, 1976.

and never dehydrated under vacuum before used. 4′-Formyl-2,2′:6′,2″-terpyridine[21] and *N*,*N*′-dihydroxy-2,3-diamino-2,3-dimethylbutane[22] were prepared according to literature procedures. Sodium periodate and selenium dioxide are commercially available.

Terpy-NIT. A solution of 4′-formyl-2,2′:6′,2″-terpyridine (415 mg, 1.59 mmol) and *N*,*N*′-dihydroxy-2,3-diamino-2,3-dimethylbutane (485.5 mg, 3.26 mmol) in MeOH (10 mL) was stirred at room temperature during 10 days. The solvent was evaporated and the crude product was oxidized under phase transfer condition with $NaIO_4$ (600 mg, 2.80 mmol) (H_2O/CH_2Cl_2) during 1.5 h. After separation and evaporation of the organic phase, the product was chromatographed over a column packed with Al_2O_3 (using a mixture of AcOEt/hexane 3/7 as eluant). The blue radical was recristallised from CH_2Cl_2−hexane to yield the pure title compound (64%). FAB^+ (*m*-NBA) 389.1 $[M + H]^+$, 373.1 [M + H − O], 358.1 [M + H − 2O]; IR (KBr pellet, cm^{-1}) 1584 (s), 1564 (s), 1541 (s), 1468 (s), 1362 (s), 1217 (m), 1127 (s), 793, (s), 657 (s); UV−vis (CH_2Cl_2) λ(nm) (ϵ ($M^{-1}cm^{-1}$)) 594 (650), 376 (35910), 283 (94370), 252 (62420), 234 (72720). Anal. Calcd for $C_{22}H_{22}N_5O_2$ (M_r = 388.45): C, 68.03; H, 5.71; N, 18.03. Found: C, 67.87; H, 5.49; N, 17.83.

Terpy-IM. A solution of 4′-formyl-2,2′:6′,2″-terpyridine (292 mg; 1.12 mmol) and *N*,*N*′-dihydroxy-2,3-diamino-2,3-dimethylbutane (250 mg, 1.69 mmol) in MeOH (25 mL) was stirred at room temperature during 4 days. SeO_2 (12.3 mg; 0.11 mmol) was added and the mixture was heated 5 h at 60 °C and then stirred at room temperature for 42 additional hours. The solvent was evaporated and the crude product was oxidized under phase transfer condition with $NaIO_4$ (295 mg; 1.38 mmol) (H_2O/CH_2Cl_2) during 1.5 h. The organic phase was separated and evaporated. The product was chromatographed over a column packed with Al_2O_3 (AcOEt/hexane 1/9). The orange radical was obtained by recristallisation from CH_2Cl_2−hexane (17%). FAB^+ (*m*-NBA) 373.1 $[M + H]^+$, 357.9 [M + H − O]; IR (KBr pellet, cm^{-1}) 1584 (s), 1564 (s), 1537 (s), 1467 (s), 1393 (s), 1263 (s), 1112 (s), 792, (s); UV−vis (CH_2Cl_2) λ(nm) (ϵ ($M^{-1}cm^{-1}$)) 477 (640), 449 (770), 427 (740), 380 (1720), 320 (27070), 280 (55510), 236 (82560). Anal. Calcd for $C_{22}H_{22}N_5O_1$+$2H_2O$ (M_r = 408.48): C, 64.69; H, 6.42; N, 17.14. Found: C, 64.55; H, 6.40; N, 17.09.

General Procedure for the Complex Preparation. A solution of 1 equiv $M(ClO_4)_2 \cdot 6H_2O$ (M = Ni, Zn, Cu) in 3 mL MeOH was added to a solution of terpy-NIT or terpy-IM (50 mg scale, 2 equivalents) in 3 mL CH_2Cl_2 The mixture was stirred during 4 to 6 h for complexes **2**-**5**, and 1 day for complex **1**. Filtered over Celite, the complex was crystallized by slow diffusion of hexane (**2**, **4** and **5**) or Et_2O (**3**). In the case of compound **1**, the solvents were evaporated and the crude solid was dissolved in CH_2Cl_2 and slow diffusion of hexane resulted in the crystallization of the desired compound.

[Ni(terpy-NIT)$_2$](ClO$_4$)$_2$ 1. 76%; FAB^+ (*m*-NBA) 933.3 $[M - ClO_4]^+$, 917.3 $[M - ClO_4 - O]$, 901.3 $[M - ClO_4 - 2O]$, 834 $[M - 2ClO_4 - H]$, 818 $[M - 2ClO_4 - H - O]$; IR (KBr pellet, cm^{-1}) 1613 (s), 1555 (m), 1469 (m), 1399 (s), 1370 (s), 1251 (m), 1099 (s), 793, (m), 621 (m); UV−vis (CH_2Cl_2) λ(nm) (ϵ ($M^{-1}cm^{-1}$)) 404 (6100), 339 (26400), 325 (29600), 283 (33750). Anal. Calcd for $C_{44}H_{44}N_{10}O_{12}NiCl_2$ (M_r = 1034.51): C, 51.09; H, 4.29; N, 13.54. Found: C, 50.92; H, 4.02; N, 13.35.

[Zn(terpy-NIT)$_2$](ClO$_4$)$_2$ 2. 99%; FAB^+ (*m*-NBA) 941.5 $[M - ClO_4]^+$, 840.3 $[M - 2ClO_4 - 2H]$, 808.3 $[M - 2ClO_4 - 2O]$, 776.2 $[M - 2ClO_4 - 4O]$; IR (KBr pellet, cm^{-1}) 1610 (s), 1550 (m), 1470 (m), 1398 (s), 1369 (s), 1252 (m), 1095 (s), 794 (m), 625 (m); UV−vis (CH_2Cl_2) λ(nm) (ϵ($M^{-1}cm^{-1}$)) 677(100), 340 (39500), 323 (41800), 287(53300). Anal. Calcd for $C_{44}H_{44}N_{10}O_{12}ZnCl_2$ (M_r = 1041.19): C, 50.76; H, 4.26; N, 13.45. Found: C, 50.58; H, 4.15; N, 13.27.

[Cu(terpy-NIT)$_2$](ClO$_4$)$_2$ 3. 99%; FAB^+ (*m*-NBA) 938.5 $[M - ClO_4 + H]^+$, 807.5 $[M - 2ClO_4 - 2O - H]$; IR (KBr pellet, cm^{-1}) 1612 (s), 1549 (m), 1471 (m), 1399 (s), 1370 (s), 1250 (m), 1096 (s), 794 (m), 625 (m); UV−vis (CH_2Cl_2) λ(nm) (ϵ($M^{-1}cm^{-1}$)) 691(170), 43(9800), 343(39150), 324(39250), 289(47400). Anal. Calcd for $C_{44}H_{44}N_{10}O_{12}CuCl_2$ (M_r = 1039.35): C, 50.85; H, 4.27; N, 13.48. Found: C, 50.85; H, 4.02; N, 13.35.

Scheme 1. Synthesis of the Complexes

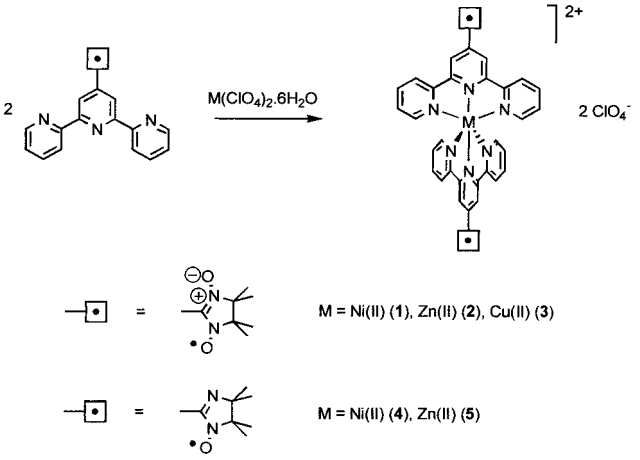

[Ni(terpy-IM)$_2$](ClO$_4$)$_2$ 4. 96%; FAB^+ (*m*-NBA) 901.3 $[M - ClO_4 - 2H]^+$, 802.3 $[M - 2ClO_4 - H]$, 770.2 $[M - 2ClO_4 - 2O]$; IR (KBr pellet, cm^{-1}) 1613 (s), 1556 (m), 1473 (s), 1417 (s), 1375 (m), 1251 (m), 1107 (s), 795 (m), 623 (m); UV−vis (CH_2Cl_2) λ(nm) (ϵ($M^{-1}cm^{-1}$)) 480(1800), 349(32900), 335(34500), 279(75450). Anal. Calcd for $C_{44}H_{44}N_{10}O_{10}NiCl_2$ (M_r = 1002.51): C, 52.72; H, 4.42; N, 13.97. Found: C, 52.57 H, 4.25 N, 13.67.

[Zn(terpy-IM)$_2$](ClO$_4$)$_2$ 5. 84%; FAB^+ (*m*-NBA) 911.3 $[M - ClO_4 + 2H]^+$, 810.3 $[M - 2ClO_4]$, 776.3 $[M - 2ClO_4 - 2O - 2H]$; IR (KBr pellet, cm^{-1}) 1611 (s), 1573 (m), 1474 (s), 1416 (s), 1374 (m), 1253 (s), 1104 (s), 795, (m), 624 (m); UV−vis (CH_2Cl_2) λ(nm) (ϵ($M^{-1}cm^{-1}$)) 498(625), 348 (31100), 337(31400), 286(39200). Anal. Calcd for $C_{44}H_{44}N_{10}O_{10}ZnCl_2$ (M_r = 1009.19): C, 52.37; H, 4.39; N, 13.88. Found: C, 52.04; H, 4.18; N, 13.49.

Results and Discussion

Synthesis. The terpy-NIT and the terpy-IM ligands have been prepared as described in a preliminary account.[23] The complexes were obtained by mixing one equivalent of the corresponding metal salt with two equivalents of the terpyridine ligand as outlined in Scheme 1.

The complex formation is accompanied by a color change from blue to green and from orange to red respectively for the terpy-NIT and terpy-IM radicals. No significative shift of the N−O stretching frequencies are observed in the IR spectrum, confirming that the radicals are not directly coordinated to the metal ion. This coordination mode is also confirmed by the crystal structures of compound **1**, **4**, and **5**. The FAB mass spectra of the complexes exhibit an intense molecular peak and several characteristic fragments due to the successive loss of oxygen atoms and/or perchlorate anion in keeping with the formulated complexes.

Structural Details. Terpy-NIT. The unit cell contains four ligands, whose ORTEP view is shown in Figure 1. The bond lengths of the radical fragment are as expected for a nitronyl-nitroxide radical [N−O = 1.27−1.28 Å, C−N = 1.34−1.35 Å]. This ring forms a dihedral angle of 24.2° with the central pyridine ring. The two external pyridine rings are transoïd to the central one and are tilted by 5.1° (pyridine N1) and 13.8° (pyridine N3), to minimize stereoelectronic interaction between the nitrogen lone pairs. Relatively short distances are found between the oxygen atom of the radical and the hydrogens of the external pyridine rings [O2−H9(C14) = 2.45 Å, O2−H8(C13) = 2.85 Å], between the oxygen atom and the hydrogens of the methyl groups of a neighboring radical [O1−

(21) Potts, K. T.; Konwar, D. *J. Org. Chem.* **1991**, *56*, 4815.
(22) Lamchen, M.; Mittag, T. W. *J. Chem. Soc. C* **1966**, 2300.
(23) Stroh, C.; Ziessel, R. *Tetrahedron Lett.* **1999**, 40, 4543.

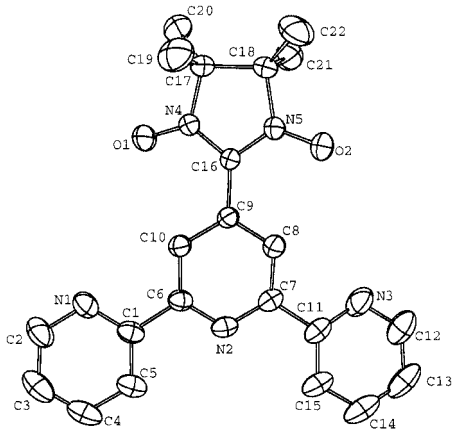

Figure 1. ORTEP view of ligand terpy-NIT.

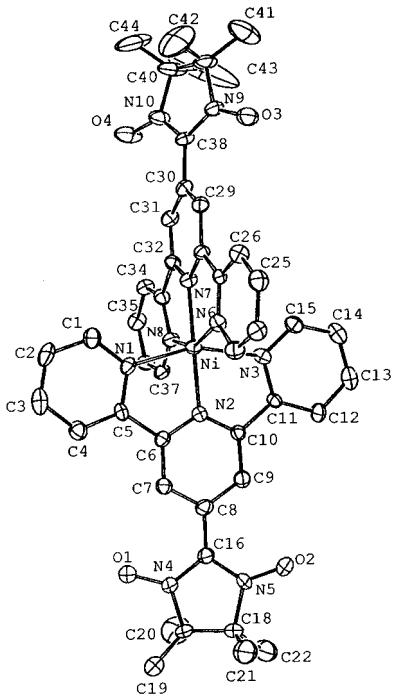

Figure 2. ORTEP view of the $[Ni(terpy\text{-}NIT)_2]^{2+}$ cation of complex **1**.

H17(C21) = 2.68 Å, O1−H20(C22) = 2.92 Å] and between the oxygen atom and a hydrogen of the central pyridine ring [O2−H6(C10) = 3.89 Å]. The distances between the NO groups of two radicals are larger than 4 Å.

$[Ni(terpy\text{-}NIT)_2](ClO_4)_2\cdot CH_2Cl_2\cdot H_2O$ (1). The unit cell contains four $[Ni(terpy\text{-}NIT)_2]^{2+}$ cations with eight uncoordinated perchlorate anions. There are also four CH_2Cl_2 and H_2O molecules. Figure 2 shows an ORTEP view of the cation. The nickel(II) cation is surrounded by two terpyridine ligands giving a distorted octahedron coordination mode with the apical Ni−N distances being shorter than the basal ones (ca. 1.98 Å and ca. 2.10 Å, respectively). Exact values are gathered in Table 2. The N1−Ni−N3 and the N6−Ni−N8 angles show important deviation from ideal octahedron (ca. 156°) due to the shape of the terpyridine ligand.

The nitronyl-nitroxide radicals are not directly coordinated to the metal ion and are located on the pyridyl fragments which occupy the apical positions. The ONCNO are nearly planar but the two radicals have different geometrical features. In the first case, the bond lengths for N4−O1, N5−O2, and C16−N5, C16−N4 (1.26 and 1.37 Å, respectively) are quite different.

Table 2. $M(terpy\text{-}rad)_2^{2+}$: Selected Bond Lengths (Å) and Bond Angles (deg) of MN_6 Polyhedron

	1	**4**	**5**
MN_1	2.070(9)	2.106(7)	2.185(4)
MN_2	1.983(9)	2.003(7)	2.092(3)
MN_3	2.129(9)	2.132(7)	2.200(4)
MN_6	2.111(8)	2.112(8)	2.179(4)
MN_7	1.983(8)	1.969(7)	2.065(4)
MN_8	2.102(8)	2.090(8)	2.130(4)
N_2MN_7	177.6(3)	178.6(3)	178.4(1)
N_1MN_3	157.0(3)	155.4(3)	151.1(1)
N_6MN_8	155.4(3)	156.8(3)	151.5(1)
N_6MN_3	88.8(3)	90.5(3)	91.9(1)
N_6MN_1	95.5(3)	94.3(3)	91.6(1)

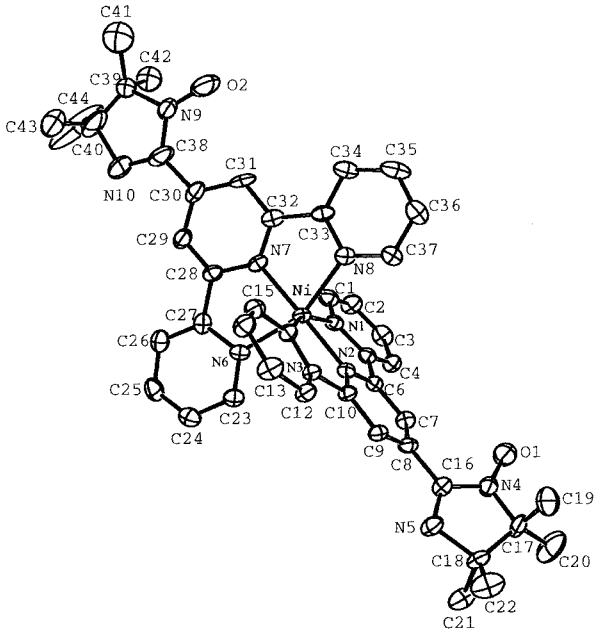

Figure 3. ORTEP view of the $[Ni(terpy\text{-}IM)_2]^{2+}$ cation of complex **4**.

The distance between the radical and the pyridyl is 1.43 Å (C16−C8) and the dihedral angle between these two cycles is 18.0°. In the second case, the bond lengths N9−O3, N10−O4, and C38−N9, C38−N10 are similar (ca. 1.30 Å and ca. 1.32 Å, respectively). Another important feature for this second ligand is the longer distance between the radical and the pyridyl C38−C30 (1.48 Å) and the dihedral angle between the pyridine and five membered ring is slightly larger (26.9°). One can also note that the torsion angles between the pyridyl rings varies from 1 to 8° and that the exocyclic bond lengths are in the range of 1.47 to 1.51 Å. Intermolecular contacts which may account for the magnetic exchange pathways have also been analysed. Indeed, the NO fragments of neighboring molecules are well separated with the shortest intermolecular distances being greater than 4 Å.

$[Ni(terpy\text{-}IM)_2](ClO_4)_2\cdot CH_2Cl_2\cdot 0.5CH_3OH$ (4). The unit cell contains one $[Ni(terpy\text{-}IM)_2]^{2+}$ cation, two uncoordinated perchlorate anions, one CH_2Cl_2 molecule One methanol molecule is shared by two unit cells. The nickel(II) is surrounded by two terpy-IM subunits providing a distorted octahedron with the apical Ni−N distances shorter than the basal ones (ca. 1.99 Å and ca. 2.11 Å respectively). The N1−Ni−N3 and the N6−Ni−N8 angles show the same deviation from ideal octahedron (ca. 156°) as in compound **1**. Figure 3 shows an ORTEP view of the cation.

The imino-nitroxide radicals are located on the pyridyl fragments which occupy the apical position and both have very

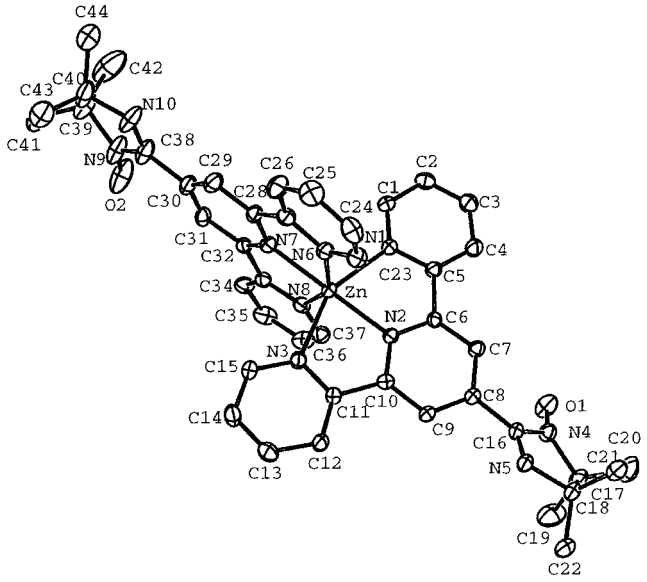

Figure 4. ORTEP view of the $[Zn(terpy\text{-}IM)_2]^{2+}$ cation of complex **5**.

different geometrical features. The bond lengths of the first radical are 1.27, 1.39, and 1.27 Å for N4−O1, C16−N4, and C16−N5, respectively. The distance between the radical and the pyridyl C16−C8 is 1.50 Å and the dihedral angle between the two cycles is 37.5°. The bond lengths of the second radical are 1.34, 1.37, and 1.33 Å for N9−O3, C38−N9, and C38−N10, respectively. The bond lengths between the radical and the pyridyl (C38−C30) is 1.45 Å and the dihedral angle between these two cycles is only 1.7°. The torsion angles between the pyridyl rings of the chelating terpyridines are ca. 2° and the bond lengths between them ca. 1.48 Å. There are no relevant intermolecular contacts which may account for intermolecular magnetic exchange pathways. Indeed, the NO fragments of neighboring molecules are distant by more than 4 Å and no short contact with the pyridyl ring bearing a radical could be found.

$[Zn(terpy\text{-}IM)_2](ClO_4)_2\cdot CH_2Cl_2\cdot 0.5CH_3OH$ (5). This compound is isostructural with **4**. The geometrical feature of the zinc(II) coordination sphere remains similar with Zn−N distances of ca. 2.08 Å and ca. 2.18 Å, respectively, for the apical and the basal positions. Exact values are given in Table 2. Here the N1−Zn−N3 and the N6−Zn−N8 angles are of the order of 151°. Figure 4 shows an ORTEP view of the cation.

There is a geometrical difference between the two tridentate ligands, with bond lengths of the first radical similar to that of compound **4** [N4−O1, C16−N4, and C16−N5 are 1.26, 1.39, and 1.27 Å, respectively]. The same bond distance between the radical and the pyridyl (C16−C8) and a similar dihedral angle between the two cycles (37.5°) is also found as for complex **4**. The second radical display a similar behavior [N9−O2, C38−N9, and C38−N10 are 1.31, 1.37, and 1.31 Å, respectively]. However, the dihedral angle between this second radical and the pyridyl ring is only 1.8°, while the distance between the radical and the pyridyl C38−C30 is slightly longer (1.48 Å). As for the two other complexes, there are no intermolecular contacts significative of magnetic exchange pathways. The shortest intermolecular distance between NO fragments is greater than 4 Å which confirmed that these complexes are merely isolated.

Magnetic Properties. Terpy-NIT. The $\chi\cdot T$ at 280K (0.378 emu·K·mol^{-1}) is slightly higher than the value required for one uncorrelated spin $^1/_2$. The magnetic behavior follows a Curie law above 20 K. By lowering the temperature below 20 K, the $\chi\cdot T$ curve decreases due to intermolecular antiferromagnetic interactions. A Curie−Weiss law (eq 1)with a Curie constant of 0.38 emu·K·mol^{-1}and a mean-field temperature $\theta = -0.3$ K has been used to fit the experimental data (Figure 5a).

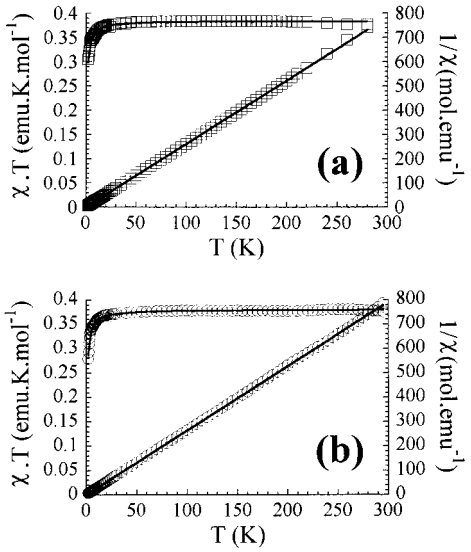

Figure 5. $\chi\cdot T$ versus T for the ligands: (a) terpy-NIT (□) and (b) terpy-IM (○).

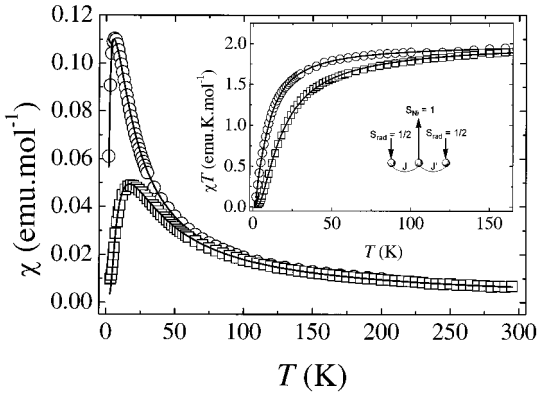

Figure 6. $\chi\cdot T$ versus T and χ versus T for the $[Ni(terpy\text{-}NIT)_2](ClO_4)_2$ complex **1** (□) and $[Ni(terpy\text{-}IM)_2](ClO_4)_2$ complex **4** (○). Insert represents an interaction scheme, for complex **1** $J = J'$.

$$\frac{1}{\chi} = \frac{T-\theta}{C} \qquad (1)$$

Terpy-IM. The value of the $\chi\cdot T$ product at 280 K (0.379 emu·K·mol^{-1}) is also slightly higher than the value required for one uncorrelated spin $^1/_2$. A plateau is observed by decreasing the temperature until 20 K. The $\chi\cdot T$ curve decreases rapidly at lower temperature according to antiferromagnetic intermolecular interactions. A Curie−Weiss law has been used to fit the experimental data, resulting in a Curie constant of 0.38 emu·K·mol^{-1} and a mean-field temperature of $\theta = -0.5$ K (Figure 5b).

$[Ni(terpy\text{-}NIT)_2](ClO_4)_2$ (1). The mean value of $\chi\cdot T$ at room temperature (1.94 emu·K·mol^{-1}) is in the range of the value expected for three uncorrelated spins: a high-spin nickel(II) ($S = 1$, $g = 2.2$) and two nitronyl-nitroxide radicals ($S = ^1/_2$) (calculated value: $\chi\cdot T = 1.96$ emu·K·mol^{-1}). By lowering the temperature, the $\chi\cdot T$ decreases slowly until ca. 50 K and more rapidly below this temperature to vanish at 2 K (Figure 6). The

$1/\chi = f(T)$ curve follows a Curie−Weiss law above 30 K with a Curie constant of 2.06 and a mean-field temperature $\theta = -15.4$ K.

This magnetic behavior indicates that antiferromagnetic interactions are predominant in the complex. According to the structural data, complex **1** is best described as isolated molecular units. Therefore, the magnetic behavior is described on the basis of linear radical−Ni(II)−radical trimer corresponding to the following spin Hamiltonian:

$$H = -2J\hat{S}_{rad}\hat{S}_{Ni} - 2J'\hat{S}_{Ni}\hat{S}_{rad} - D\left(S_{Ni}^{Z\,2} - \frac{2}{3}\right) - (2g_{rad}\hat{S}_{rad} + \bar{g}_{Ni}\hat{S}_{Ni})\mu_B\vec{H} \quad (2)$$

where J and J' hold for the exchange interaction coupling between the nickel(II) ion and the two terpy-NIT ligands, $\hat{S}_{rad}$ is the spin operator for the radicals ($S = {}^1/_2$), $\hat{S}_{Ni}$ the spin operator for the nickel(II) ion ($S = 1$), D is the zero field splitting for octahedral Ni(II). The isotropic g factor for the radicals was fixed at $g_{rad} = 2.003$ while for the nickel cation $\bar{g}_{Ni}$ has to be decomposed in its parallel and perpendicular components, g_{Ni}^{Z} and g_{Ni}^{xy} respectively, to account for the zero field splitting effect on the parallel (χ^z) and perpendicular (χ^{xy}) parts of the susceptibility. No analytical expression was found in the open literature, however the total magnetic susceptibility of the compound, $\chi = 1/3(\chi^z + 2\chi^{xy})$, was determined from the above Hamiltonian by numerical diagonalization of the corresponding 12×12 exchange matrix expressed on the basis set of all the magnetic states of the system.[24] Comparison with the experimental measurements was carried out by using the minimization program MINUIT.[25] When all the parameters are kept free, a very good fit is obtained between calculated and experimental susceptibility resulting in comparable values for $2J$ and $2J'$ (≈ -20 K), in agreement with the structural findings, and isotropic nickel g factor ($g_{Ni}^{Z} \approx g_{Ni}^{xy} \approx 2.2$). However, various D values are obtained depending strongly on the initial value chosen before starting the refinement. This clearly indicates that the experimental behavior is not much affected by the zero field splitting compared to the magnetic exchange interaction. To avoid any over-parametrization of the system another set of fittings parameters was tested. The D value has been assumed to be the same as found by Waldmann et al. for the parent $[Ni(terpy)_2](PF_6)$ compound[26] fixed at +9 K,[27] and an isotropic g factor was used as deduced from EPR measurements (vide infra). Then, the best fit is obtained for $2J = -19.7 \pm 0.5$ K, $2J' = -19.5 \pm 0.5$ K and $g_{Ni} = 2.26 \pm 0.08$. The agreement with the experience is well-illustrated in Figure 6.

$[Zn(terpy\text{-}NIT)_2](ClO_4)_2$ (2). The value of $\chi \cdot T$ (0.65 emu·K·mol^{-1}) at 300 K is quite lower than the expected value for two uncorrelated spins ($\chi \cdot T = 0.75$ emu·K·mol^{-1}). However, by analogy with compound **5** (see below), it is suggested that solvate molecules in the crystal structure of the compound are responsible for the underestimation of the diamagnetic contribution. The lack of data around 50 K is due to the exact balance between the diamagnetic contribution and the paramagnetic one.

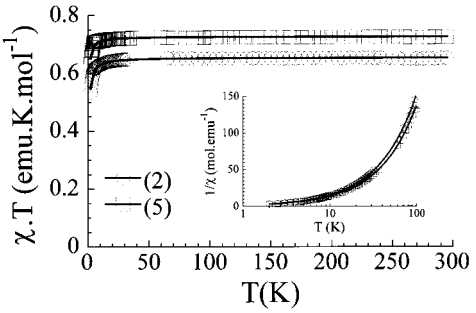

Figure 7. $\chi \cdot T$ versus T for the $[Zn(terpy\text{-}NIT)_2](ClO_4)_2$ complex **2** (○) and $[Zn(terpy\text{-}IM)_2](ClO_4)_2$ complex **5** (□). Insert: $1/\chi$ versus log(T).

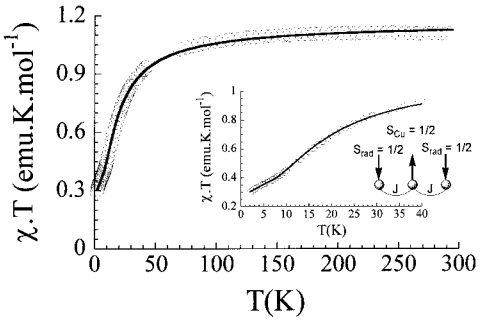

Figure 8. $\chi \cdot T$ versus T for the $[Cu(terpy\text{-}NIT)_2](ClO_4)_2$ complex **3**. Insert shows the 0−40 K part of the susceptibility measurements. Insert represents an interaction scheme.

This effect is responsible for the vanishing signal output for the total SQUID response. The resulting magnetization is then much affected by fluctuations. The $\chi \cdot T$ curve exhibit a plateau above 50 K and then drops sharply at lower temperature. This behavior is typical of predominantly antiferromagnetic interactions (Figure 7).

These are attributed to intermolecular interactions because of the estimated very small interaction between the two radicals of the complex as found by EPR measurement (vide infra). A good fit of the susceptibility data over the whole range of temperature is obtained using a Curie−Weiss law, with a Curie constant of C = 0.7 emu·K·mol^{-1} and a mean-field temperature $\theta = -0.4$ K (Insert in Figure 7).

$[Cu(terpy\text{-}NIT)_2](ClO_4)_2$ (3). The $\chi \cdot T$ product at room temperature (1.1 emu·K·mol^{-1}) is close to the expected value for three uncorrelated $S = {}^1/_2$ spins (calculated value: 1.125 emu·K·mol^{-1}). The overall behavior of $\chi \cdot T$ reflects antiferromagnetic interactions as expected for this kind of Cu(II) complexes. The explanation for the missing data around 50 K has been previously detailed. If one assumes that the complex is magnetically isolated as found for the related Ni(II) and Zn(II) complexes, the $\chi \cdot T$ curve should level off at ca. 0.375 emu·K·mol^{-1} at low temperature for such a three spin ${}^1/_2$ system. By careful examination of the shape of this curve, one can note a shoulder near this value, followed by a continuous decrease due to weak intermolecular interactions (Figure 8).

The experimental data are parametrized by a model consisting of an isocele triangle,[28] weakly coupled through a mean-field interaction. By assuming that the intermolecular radical−radical interaction is zero ($J' = 0$) this model indeed correspond to a linear three spins system. The following fit values are obtained: Cu−NIT interaction $2J_{Cu-NIT}/k_B = -22.8$ K with $g = 2.03$, together with a mean-field temperature $\theta = -0.5$ K. It is

(24) The diagonalization is performed with rsm, a subroutine for finding eigen values and eigen vectors of symmetrical matrixes, involved in the FORTRAN library EISPACK.
(25) MINUIT, a function minimization program, CERN Program Library Entry D506, Geneva, Switzerland.
(26) Waldmann, O.; Hassmann, J.; Müller, P.; Volmer, D.; Schubert, U. S. and Lehn, *J.-M. Phys. Rev. B*, **1998**, *58*, 3277.
(27) Compared to ref 26 the opposite sign of D corresponds to opposite sign in the Hamiltonian.
(28) Belorizky, E. J. *Phys. I France* **1993**, *3*, 423.

worth noting that an asymmetric linear three spin system yields also a good correlation but providing a higher uncertainty on the exchange interaction parameters.

[Ni(terpy-IM)$_2$](ClO$_4$)$_2$ (4). The value of the $\chi \cdot T$ product at high temperature (2.09 emu·K·mol^{-1}) is near the value expected for uncorrelated spins in the case of a high-spin nickel(II) ($g = 2.2$) and two nitronyl-nitroxide radicals (calculated value: $\chi \cdot T = 1.96$ emu·K·mol^{-1}). By decreasing the temperature down to 50 K, the curve decreases very slowly. Below 50 K, the $\chi \cdot T$ product decreases more sharply approaching zero at very low temperature. The $1/\chi$ versus T curve follows a Curie−Weiss law above 15 K with a Curie constant of 2.18 and a mean-field temperature $\theta = -10.0$ K. According to the structure, this compound may be descibed as an assembly of quasi-isolated magnetic radical−Ni−radical trimers. The experimental susceptibility was fitted with the same model as used precedently for complex **1**. Similarly, and for the same reasons, the fixed value $D = +9$ K and isotropic g factor for the Ni(II) ion has been assumed. The best agreement between experimental and calculated suceptibility is obtained with $2J = -5.6 \pm 0.3$ K, $2J' = -13 \pm 0.4$ K and $g_{Ni} = 2.24 \pm 0.08$. The fit with the experience is illustrated in the Figure 6.

[Zn(terpy-IM)$_2$](ClO$_4$)$_2$ (5). As for compound **2**, the correction with the molecular weight of the compound gives only a $\chi \cdot T$ of 0.65 emu·K·mol^{-1}. By taking into account the solvate molecules present in the crystal structure, the proper diamagnetic correction yields $\chi \cdot T = 0.72$ emu·K·mol^{-1} which is in good agreement with the expected value for two uncorrelated spins ($\chi \cdot T = 0.75$ emu·K·mol^{-1}) (Figure 7). Qualitatively, the same behavior is observed as for complex **2**. Therefore, a similar procedure has been used to fit the data using a Curie−Weiss law with C = 0.7 emu·K·mol^{-1}, and $\theta = -0.2$ K (Insert in Figure 7).

EPR Spectra. The EPR spectra were recorded at room temperature for diluted and degassed solutions (ca. 10^{-4} M in CH_2Cl_2) for the five complexes. EPR measurements of the powder were recorded at 4, 10, 20, 50, and 100 K. The hyperfine pattern observed for the complexes in solution at room temperature are very different from one another. Compound **1** [Ni(II)(terpy-NIT)$_2$] is EPR silent in dilute solution at room temperature, whereas its IM derivative homologue **4** [Ni(II)-(terpy-IM)$_2$] exhibits the 7 lines pattern of a residual IM monoradical. This can be attributed to traces of ligand or uncoupled radical. Because unsubstituted terpyridine ligands formed very stable complexes in the presence of various transition metal salts including Zn^{2+}, Cu^{2+}, and Ni^{2+} (Log $K = 21.8$),[29] it is surmized that the observation of a residual signal is most probably due to uncoupled radical subunits. For **2** [Zn(II)(terpy-NIT)$_2$] and **5** [Zn(II)(terpy-IM)$_2$], both spectra are symmetric and contain more lines than expected for a monoradical (5 lines pattern for NIT). The observed pattern is even more complex than expected for a biradical in the strong exchange limit (9 lines for bis-NIT or 13 lines for bis-IM), i.e., when the intramolecular exchange interaction J' is much larger than the hyperfine coupling constant, a: $J' \gg a$.[30] The hyperfine interaction with the ^{67}Zn nucleus ($I = {}^5/_2$) is not observed, due to the low natural abundance (4.1%) of this isotope. The complex pattern is spanning over a broader field range than expected for a typical single radical. It must be related to the intermediate exchange regime, i.e., when $J' \approx a$.[31] In such a case, additional lines may be observed in the EPR spectrum. Moreover, the observation of some outer extra lines corresponding to peculiar transitions allows for a rough estimation of the absolute value of the exchange interaction.[29a,32] In the case of complex **2**, the spectrum is centered at $g = 2.0067$, as expected for a NIT radical derivative (Figure 9a).

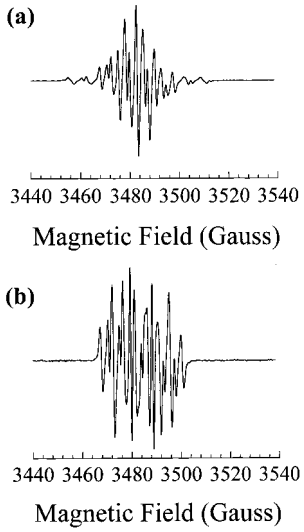

Figure 9. (a) EPR solution spectra at room temperature for the [Zn-(terpy-NIT)$_2$](ClO$_4$)$_2$ complex **2**. (b) EPR solution spectra at room temperature for the [Zn(terpy-IM)$_2$](ClO$_4$)$_2$ complex **5**.

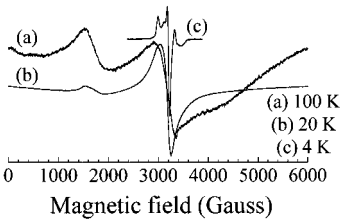

Figure 10. EPR powder spectra forthe [Ni(terpy-NIT)$_2$](ClO$_4$)$_2$ complex **1** (a) at 100 K, (b) at 20 K, and (c) at 4 K.

The exchange coupling constant can be estimated as:

$$|J'| = \frac{\Delta H - a^2}{\Delta H} \qquad (3)$$

where ΔH is the distance between the outer lines and the center of the spectrum, and a the hyperfine interaction, with a magnitude being of the order of a few mK. This affords estimations of $|J'|$ of the order of 5 mK for **2** and of 1 mK for **5** for which $g = 2.0060$, as expected for an IM radical derivative (Figure 9b). For **3** [Cu(II)(terpy-NIT)$_2$], the same feature as in **2** and **5** is observed. The observation of the outer transitions affords an exchange coupling constant similar as for **2**. From 100 K down to 20 K, complex **1** exhibits a two lines spectrum superimposed to a very broad background feature extending over the whole field scan. The main component of the observed two peaks at room temperature is featureless and centered at 2.14, whereas the other component corresponds to a weak half-field resonance close to 1530 G (Figure 10a).

(29) Holyer, R. H.; Hubbard, C. D.; Kettle, S. F. A. and Wilkins, R. G. *Inorg. Chem*. **1966**, *5*, 622. Kim, K. Y.; Nancollas, G. H. *J. Phys. Chem*. **1977**, *81*, 948.

(30) (a) Luckhurst, G. R. In *Spin Labeling. Theory and applications*; Berliner, J. L., Ed.; Academic Press: Cambridge, MA, 1976; p 133. (b) Luckhurst, G. R.; Pedulli, G. F. *J. Am. Chem. Soc*. **1970**, *92*, 4738.

(31) (a) Brière, R.; Dupeyre, R.-M.; Lemaire, H.; Morat, C.; Rassat, A.; Rey, P. *Bull. Soc. Chim. France* **1965**, 3290. (b) Glarum, S.; Marshall, J. H. *J. Chem. Phys*. **1967**, *47*, 1374.

(32) Metzner, E. K.; Libertini, L. J.; Calvin, M. *J. Am. Chem. Soc*. **1977**, *99*, 4500.

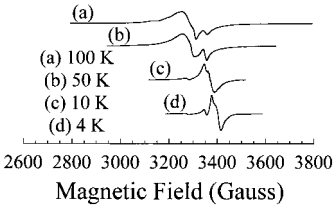

Figure 11. EPR powder spectra forthe $[Cu(terpy\text{-}NIT)_2](ClO_4)_2$ complex **3** (a) at 100 K, (b) at 53 K, (c) at 10 K, and (d) at 4 K.

The line width of the main line decreases as the temperature decreases from 450 G at 100 K down to 220 G at 20 K. A much narrower component is guessed within this line as it drops abruptly at the resonance, even exhibiting an apparent narrow peak at 100 K (Figure 10a). This narrow signal is attributed to the nitronyl-nitroxyde radical, whereas the other two components, i.e., the half-field line and the $g = 2.15$ line must be attributed to the triplet signal of Ni(II) in an octahedral field.[33] The intensity of the various components of the EPR signal increases with decreasing temperature down to 20 K. According to the susceptibility data, the signal drops rapidly to 0 below ca. 20 K. As suggested in the study of **4** in solution, the remaining feature observed at 4 K must be attributed to a low fraction of uncoupled ligand together with the resulting Ni(II) ions in a low symmetry environment as revealed by the anisotropic powder spectrum (Figure 10c). The behavior of compound **4** as probed through EPR is quite similar to the one depicted for compound **1**. As in **1**, a two components signal is attributed to octahedral Ni(II). The main difference is that the single line signal of the radical is much more peaked than observed in **1**. It corresponds to the signal of an imino-nitroxyde radical submitted to exchange interaction within a solid,[34] with $g = 2.0066$ and a peak-to-peak line width, $\Delta B_{pp} = 6.8$ G. These observations are in agreement with the magnetic behavior of **1** and **4** as discussed from the susceptibility data.

The powder spectra of complex **2** show an isotropic signal centered at $g = 2.0069$ with $\Delta B_{pp} = 9.0$ G, typical of a nitronyl-nitroxide radical. The position and the width of the resonance remain unchanged by lowering the temperature down to 4 K. A weak half-field signal centered at $g \cong 4.01$ is detected between 4 and 50 K. Compound **5** follows a very similar behavior over the whole range of temperature with $g = 2.0064$ and $\Delta Bpp = 9.5$ G, characteristic of an imino-nitroxide radical, together with a weak half-field band centered at $g = 4.009$. These results are in agreement with the susceptibility data indicating for both compounds a weak intermolecular isotropic exchange coupling between radical spins. The occurrence of a half-field signal may be attributed to the presence of an intramolecular exchange within the biradical complexes.

At 100 K, the powder spectrum of compound **3** revealed the interaction between Cu(II) and the NIT radical (Figure 11a), as previously found in a spin-labeled complex of Cu(II) with terpyridine.[35]

Poorly resolved hyperfine coupling is observed superimposed to a broad line. A weak satellite signal is observed at $g = 2.0061$. It is attributed to uncoupled ligand, as previously discussed for the solution of compound **3**. The feature of the signal of this complex is that of an axial system with $g_{||} = 2.099$ ($a_{||} \cong 65$ G) and $g_{\perp} = 2.047$, resulting in $g_{av} = 2.082$. As the temperature decreases, the hyperfine pattern disappears due to averaging through exchange interaction. A featureless single line with $\Delta Bpp = 51$ G is observed together with the radical component at 50 K (Figure 11b). The overall shape of the signal is strongly modified at lower temperature, although the single line of the organic radical is still observed at $g = 2.006$. At 10 K and at 4 K (Figure 11c,d), the signal of the complex consists of two main lines. One of these is centered at $g = 2.05$, close to the original perpendicular component of the former Cu(II) complex. The other one is a high field line comprising different unresolved features centered at $g = 1.98-1.99$. Such a behavior may be due to a change in the symmetry of the Cu(II) ion. It is worthwhile pointing out that the susceptibility shows a shoulder below 10 K (Figure 8). However, such a behavior cannot be discussed properly with the lack of structural data at low temperature. Another possibility is the observation of fine structure within the quartet spin state that the three spins $^1/_2$ do represent, although the quartet ground state is not the ground state. As in the Ni(II) derivatives, the EPR signal is strongly affected within the temperature range comparable to the exchange interaction. This is actually an evidence for the radical−metal ion interaction.

Complexes **1**, **3**, and **4** exhibit weak intramolecular antiferromagnetic interactions between the metal ion and the nitroxide radicals. The magnetic behavior of all compounds may be simulated with the help of a linear three-spins system, since the use of a triangle model actually results in the vanishing of the third interaction. For compound **1**, the magnetic interaction values obtained are slightly higher but in good agreement with those expected for an interaction between a Ni(II) and a nitronyl-nitroxide via a pyridyl ring. It is worth noting that the use of an asymmetric model for complex **1**, does not improve significantly the refinement of the experimental data, due to the weakness of the exchange interactions. In the case of complex **4**, the fit of the data may be obtained with an asymmetric linear system. This is in agreement with the X-ray crystallographic structure, which reveals the marked asymmetry in the radical−pyridyl dihedral angles. In fact, the structure reveals that one radical is nearly planar with the terpyridine while the second is twisted by an angle of 37.5°, giving rise to different strengths of interactions. The magnetic behavior of complex **3** has been modeled on the basis of isolated symmetric or asymmetric linear magnetic trimers. However, the absence of X-ray crystal structure determination does not allow to discriminate between almost equally relevant fitting of the experimental data. A Curie−Weiss law has been used to represent the magnetic behavior of the complexes of the diamagnetic Zn(II) metal (**2** and **5**). This is a qualitative way to depict the antiferromagnetic intermolecular interactions in these compounds, since the EPR experiments confirm the presence of a very weak exchange interaction between the organic radicals across a pyridyl−Zn(II)−pyridyl moiety. The presence of uncoupled ligand has been detected in almost all of the compounds, both in solution and in the solid state. This is not surprising, since the five membered ring of the radical may be twisted with respect to the pyridyl units. Such a twist is well-known to result in the loss of through-bond exchange interaction within meta-phenylene based biradicals.[36] The fact that a strong magnetic interaction between the radical connected in the 4′-position of the terpyridine chelate and the paramagnetic metal

(33) Abragam, A.; Bleaney, B. *Electron Paramagnetic Resonance of Transition Ions*; Clarendon Press: Oxford, U. K., 1970; p 449.
(34) Stanger, J.-L.; André, J.-J.; Turek, P.; Hosokoshi, Y.; Tamura, M.; Kinoshita, M.; Rey, P.; Cirujeda, J.; Veciana *J. Phys. Rev. B* **1997**, *55*, 8398.
(35) Halcrow, M. A.; Brechin, E. K.; McInnes, E. J. L.; Mabbs, F. E.; Davies, J. E. *J. Chem. Soc., Dalton Trans*. **1998**, 2477.
(36) (a) Silverman, S. K.; Dougherty, D. *J. Phys. Chem*. **1993**, *97*, 13273. (b) Borden, W. T.; Iwamura, H.; Berson, J. A. *Acc. Chem. Res*. **1994**, 109.

center is in keeping with a good blending of the SOMO orbital of the radical and the magnetic orbitals of the metal. A related effect has been found during triplet energy transfer from a donor to an acceptor in the so-called molecular scale wires approach.[37] Further examples of transition metal complexes of terpyridine ligands grafted in various substitution positions with this kind of radicals are needed to give a deeper insight into the nature of the mechanism involved in the magnetic exchange pathways.

(37) Ziessel, R.; Hissler, M.; El-ghayoury, A.; Harriman, A. *Coord. Chem. Rev.* **1998**, *178*−*180*, 1251 and references therein.

Acknowledgment. This work was supported by the Centre National de la Recherche Scientifique, by the Engineering School of Chemistry (ECPM). Mr. M. Bernard is gratefully acknowledged for invaluable assistance in the EPR experiments and data processing, Dr. M. Drillon, Prof. E. Belorizky and Dr. P. Rey for helpful discussions, Mr R. Poinsot and A. Derory for magnetic measurements, Dr. A. De Cian and N. Kyritzakas for X-ray data acquisition and refinement.

IC001473+